Cycles in oceanic teleconnections and global temperature change.

Knut L. Seip and Øyvind Grøn

OsloMet- Oslo Metropolitan University; Faculty for Technology, Art and Design

Pilestredet 35, POB 4 St. Olavs plass N-0130, Oslo, Norway

E-mail knut.lehre.seip@oslomet.no; oyvind.gron@oslomet.no

Abstract

Three large ocean currents are represented by proxy time series: the North Atlantic oscillation, NAO, the Southern oscillation index, SOI, and the Pacific decadal oscillation, PDO. We here show how proxies for the currents interact with each other and with the global temperature anomaly, GTA, applying a novel method which identifies running average leading lagging, LL- relations, between paired series. We find common cycle times for paired series of 6 - 7 years and 25 - 28 years and identify years when LL- relations switch. Switching occurs with **XXX** 20 years interval for the short 7 years cycles and with 27± 15 years intervals for the 25-28 years cycles. During the period 1940 – 50, the LL- relations for the long cycles were circular (nomenclature x leads y: x → y): GTA → NAO → SOI → PDO → GTA. However, after 1960, the LL- relations become more complex and there are indications that GTA leads both NAO and PDO. The switching years are related to ocean current tie points and reversal points reported in the literature.

1. INTRODUCTION

Recently, it has been suggested that there are strong relationships between variables that describe water movements in the oceans and regional or global climate change. Climate model simulations, Meehl et al. (2011) and Trenberth (2015), suggest that heat is being stored in the deep ocean, e.g, the Pacific ocean (660 10^6 km^3) during pauses in temperature increase, the so called hiatus periods. Others give a prominent role to the Atlantic ocean (310 10^6 km^3) and the Atlantic meridional overturning circulation, e.g., Bryden et al. (2005) McCarthy et al. (2015), Caesar et al. (2018) and Thornalley et al. (2018). Based on these suggestions we examine leading and lagging relationships between three potential water movement variables: the North Atlantic Oscillation, NAO, The Pacific decadal oscillation, PDO, and the Southern oscillation index, SOI. We compare cycle length, phase shifts and leading – lagging, LL- relations to global temperature change, as Global temperature anomaly, GTA. However, although the three variables are used extensively as proxies for heat transfer between regions, they are only indirect measures of heath transfer.

We examine possible causal relations in long term (1880-2014) and shorter term, multidecadal and decadal, perspectives. In the decadal and multidecadal perspective we examine "before" and "after" relationships for (quasi-) oscillatory movements. To be a causal agent the cause has to come before the effect. On the other hand, if the candidate causal variable peaks after the target variable, this weakens the causality hypothesis. For cyclic phenomena, the leading – lagging, LL- statement can be interpreted as a requirement for the peak (or the trough) of a causal agent to come before the peak (or the trough) of the effect. Since the sign of the variables is arbitrary, it may be convenient to change the sign of some variables based on knowledge of the studied system and on anticipation of what the LL- relations will express. We examine two "versions" of each time

series, i) the raw time series and ii) series smoothed to identify decadal or multidecadal patterns. However, leading – lagging signatures may also result from other mechanisms than causal relations (Granger 1969). This will be examined in the discussion section.

Hypotheses. We propose three hypothesis for the relationships between GTA and ocean oscillation variables. i) *Firstly*, the large ocean currents, or their proxies, will impact each other in a concerted sequence throughout our study period 1880 – 2014, that is, the teleconnection hypothesis is supported. ii) *Secondly*, global temperature change, in particular the hiatus periods, will be associated with particular changes in the ocean current's leading, lagging, LL- relations. iii) *Thirdly*, common cycle times for paired variables will correspond to cycles that are found in both of the single variables that contribute to the pair

The rest of the paper is organized as follows. In Section 2 we present the global warming variables, in Section 3 we present methods for i) pretreating the data, ii) quantifying running average leading-lagging relations, iii) smoothing the data and iv) a Monte Carlo method that gives uncertainty estimates. In Section 4, we present the results and in Section 5, we discuss relationships between GTA and proxies for ocean currents. In Section 6, we summarizes the results.

2. MATERIALS

The global temperature series. We use the GISS Global land – ocean temperature Index in 0.01 degrees Celsius from NASA's

Goddard institute for space studies, NASA(GISTEMP) (2014). The series are updated every month and may change within their margin of error (R. Ruedy personal communication, 2014). For this series Zhen-Shan and Xian (2007) and Mazzarella and Scafetta (2012) both found that during the period 1880 to 2009 GTA has dominating cycle lengths of 6-8 years, 20 years and 60 years. White and Cayan (1998) and Keeling and Whorf (1997) found cycle lengths of 2-13 years. The data were taken from the web site: http://data.giss.nasa.gov/modelforce/ghg ases/GHGs.1850-2000.txt.

The hiatus periods. There are two periods with little and no warming in the global temperature index. Here we use the periods suggested by Trenberth (2015) and Meehl et al. (2014). The first of these, 1943 to 1975 is called the big hiatus, and the last hiatus period runs from about 1998 to 2014. It is probably also relevant to define a hiatus period from 1902 to 1920. We introduce a variable for the hiatus periods, setting it to 1 during the hiatus periods and to zero elsewhere. We also identify hiatus periods by smoothing the GTA series 1880 to 2015 and calculating the 1st derivative with respect to time. The hiatus periods are those periods where the slopes (β – coefficients) are in the negative, or small, slope tail of the slope distribution. The two first hiatus periods are included in the tails, but not the last. However, we use all three periods.

The oscillation series are proxies for oscillations that occur in wind stress, water movements, heath transfer and

regional temperature anomalies. There will most probably be mechanisms that disturb concerted oscillations in these variables, and there may be phase shifts between them. In the following, we use the term "ocean oscillation variables" for the three oscillating patterns described below.

The North Atlantic oscillation index measures the air pressure difference between a Southern station, e.g., Lisbon and the Northern station, Reykjavik ($p_{Lisbon} - p_{Reykjavik}$). We use monthly NAO index values as reconstructed by Luterbacher et al. (2002) and obtained from the web site: ftp://ftp.ncdc.noaa.gov/pub/data/paleo/historical/north_atlantic/nao_mon.txt. When the NAO index exhibits an increasing trend, European Winter time temperatures are frequently higher than normal, Hurrell (1995), McCarthy et al. (2015).

The Southern oscillation index, SOI, or the El Niño Southern Oscillation, the ENSO. The Southern Oscillation Index, SOI, is a standardized index based on the observed sea level pressure differences between Tahiti and Darwin, Australia ($p_{Tahiti} - p_{Darwin}$). The ENSO also have an oceanic component measured as the sea surface temperature in the equatorial Pacific (Kestin et al. 1998). Prolonged periods of negative SOI values coincide with abnormally warm ocean waters across the eastern tropical Pacific, typical of El Niño episodes, and positive values of the SOI show the opposite, (La Niña). Typically, temperature anomalies happen at irregular intervals of 2 to 8 years (Kestin et al. 1998). The El Niño was exceptionally strong during the period 1997 /1998 (McPhaden 1999). The data were obtained from the web site: http://www.bom.gov.au/climate/current/soihtm1.shtml

The Pacific decadal oscillation, PDO, is closely related to the interdecadal Pacific oscillation, IPO, but has a more northern hemisphere focus, (Gehne et al. 2014); Trenberth (2015). PDO is measured by the PDO index that is the leading empirical orthogonal function (EOF) of monthly sea surface temperature anomalies (SSTA) over the North Pacific after the global mean SST has been removed (poleward of 20° N, south of 65° N and between Asia and the west coast of North America). A positive IPO is related to an increase in mean sea level pressure, SLP, in the South Pacific region west of 170°W (Salinger et al. 2001). IPO shows reversals in 1925, 1947 and 1997 (Wu et al. 2011). Models show that a negative phase of the PDO (IPO) is characterized by cooler-than-normal average surface temperatures over the tropical Pacific, with opposite sign anomaly in the northwest and southwest Pacific (data from the years 2000 -2014). Positive phases of the PDO are characterized also by weaker trade winds that allow less heat to be mixed into subsurface waters and therefore cause an increase in global average surface temperature, Meehl et al. (2014), Trenberth and Fasullo (2013). The data were obtained from the web site: http://www.atmos.washington.edu/~mantua/abst.PDO.html)

The data for CO_2 were only used to show its relation to GTA. The data were obtained from the web site: http://data.giss.nasa.gov/modelforce/ghgases/GHGs.1850-2000.txt

The five variables are depicted in their raw format in Figure 1a. Figure 1b shows the five variables after detrending, smoothing and normalizing to unit standard deviation. The figures will be explained further in the method section.

Ocean currents in the Atlantic ocean are also monitored by two addional measures, the Atlantic meriodional overturning circulation, AMOC and the Atlantic multidecadal oscillation, AMO.

The AMOC is a measure of water transport, measured in Sverdrups (1Sv = 10^6 m^3 s^{-1}), zonally along a across a transect (e.g. 24.5°N) from the African coast to the Bahama islands. It is shown to be slowed by about 30% between 1957 and 2004 (Bryden et al. 2005). Several studies suggest that changes in the AMOC influences global warming (Zhang and Wang 2013; Duchez et al. 2014; Lynch-Stieglitz 2017). The AMO is defined in several ways. It is the detrended area weighted sea surface temperature, SST, from the Atlantic west coast to the eastern coast and from 0°N to 60° N. The time series for NAO, AMOC and AMO are shown in supplementary material 1.
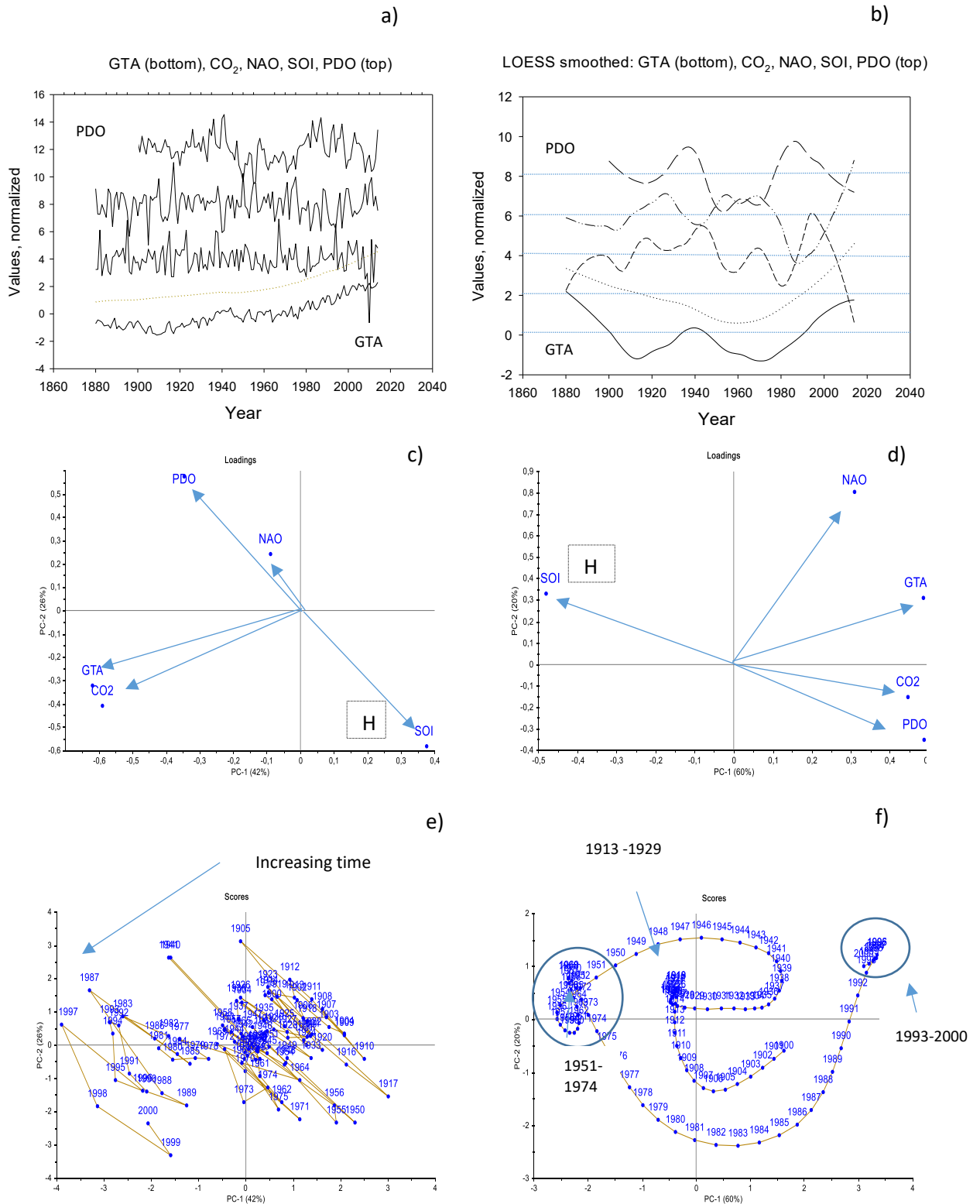
Figure 1. Global warming variables: Global temperature anomaly, GTA, Carbon dioxide, CO_2, North Atlantic oscillation, NAO, Southern oscillation index, SOI and Pacific decadal oscillation, POD. a) Raw data, shifted vertically. b) Data smoothed with the LOESS smoothing algorithm, f = 0.3, p = 2, and shifted vertically. c) Principal component plot, (loading plot) for raw, detrended variables 1900 - 2000, d) Principal component plot, (score plot) for

smoothed, detrended variables 1900 – 2000. e) score plot corresponds to c. f) score plot corresponds to d. Arrow in c indicates trajectory direction, arrows in f shows cluster of years. H indicates position of the Hiatus variable. See text

3. METHODS

In this section, we first describe pretreatment of our data. Thereafter we describe a relatively novel method for quantifying leading and lagging LL-relations. Thirdly, we discuss the rationale for smoothing the data and our choise of smoothing prameters. Finally, we describe the method used to estimate uncertainty.

3.1 Data pretreatment

We first detrend the data by calculating the residuals from a linear regression of the variables against time. Thereafter, we identify decadal and multidecadal cycles for the five time series GTA, CO_2, NAO, SOI and PDO using the LOESS smoothing algorithm (to be described in section 3.3). The parameters for the LOWESS smoothing are f = 0.3 and p = 2. Lastly, we normalize the variables to unit standard deviation. The results are shown in Figure 1b. The next figures show principal component, PCA, score plot, c, and loading plot, e, for the raw, detrended series. Results for the smoothed series are shown in d and f. All plots are restricted to the period 1900 - 2000 to avoid end effects from the smoothing algorithm, and because the first 20 years of observation may be more uncertain than the data after the 1900.

3.2 Quantifying running average phase shifts for pairs of variables

The method has previously been described in Seip and Grøn (2017). Here we give a short summary which allows the method to be copied and applied. The basis of the method is the dual representation of paired cyclic time series, x(t) and y(t), as time representation (the x-axis represents time and the two series are depicted on the y-axis) and as phase plots where the paired time series are depicted on the x-axis and the y-axis on a 2D graph (a scatter plot). If one series leads another with less than ½ a cycle length (for example by having a causal effect on the other), then we will have a persistent rotational direction of the series trajectories in the phase plot. Figures 2a and b give an example with two sine functions

(1) x (t) = SST = sine (t) ; y (t) = Sun = sine (t + π/4).

To choose a well-known example of leading and lagging variables, we let the first series, x(t), represent sea surface temperature, SST, normally peaking in July – August on the western hemisphere, denoted SST in the graph. The second series, y(t), could represent Sun insolation peaking in June. Since Sun insolation is associated with heat transfer to the sea surface, t is a candidate cause forSST. Thus, it should peak before SST, as it does

in the figure. Real pairs of Sun insolation and SST do the same (Seip 2015).

With series for SST (x- axis) and Sun insolation (y- axis) normalized to unit standard deviation, the trajectories will form an elliptic form centered in the origin and with the long axis either in the 1:1 direction or in the 1, -1 direction. Trajectories in the phase plot will rotate clock-wise, Figure 2b. If the candidate cause had come after the target, with SST still on the x-axis and Sun still on the y-axis, the rotation would be counter clock-wise.

a)

Candidate cause +0,785 and target

b)

Phase plot: Candidate cause + 0.785 and target

c)

Random, uniformly distributed time series;
positive = counter clock-wise rotations
negative = clock-wise rotations

d)

Random series as phase plot
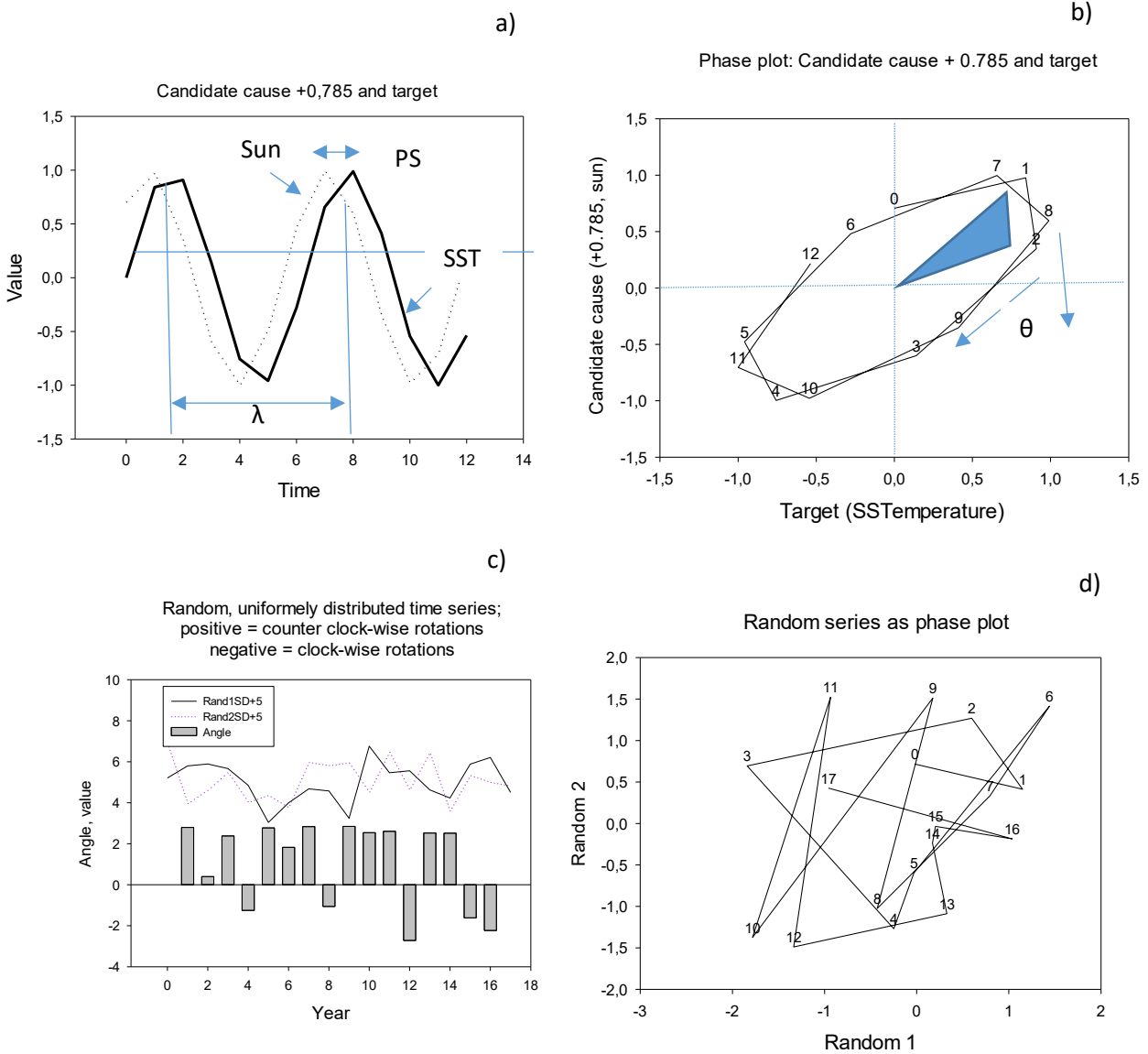
Figure 2. Relation between time series and phase plot. a) The candidate cause, Sun, peaks before, and close to the target, SST. They could represent sun insolation (cause) and sea surface temperature, SST, (effect). b) Phase plot for Sun and SST (target,SST, on x –axis); c) two uniformly random time series (upper series); bars (lower part) show the angles θ as positive and negative bars. The angle θ is measured by Eq. (5) in the main text. Note that when ∑ θ ≈ 2π, a circle-like curve is closed and the number of time steps used to close the

curve corresponds to the common cycle time of the two contributing time series; d) Phase plot for paired uniform series.

LL- relations. To see which variable peaks first, we quantify rotational directions and apply a LL- strength measure that expresses the persistence of one rotational direction for the trajectories in the phase plot for the paired time series. The formula for quantifying the rotational direction, θ, is,[1]

$$(2) \qquad \theta = sign(\mathbf{v}_1 \times \mathbf{v}_2) \cdot \text{Arccos}\left(\frac{\mathbf{v}_1 \cdot \mathbf{v}_2}{|\mathbf{v}_1||\mathbf{v}_2|}\right).$$

The strength, LL - strength, of the mechanisms that cause two variables to either rotate clock-wise or counter clock-wise in a phase portrait is measured by the number of positive rotations (counter clock-wise rotations by convention) minus the number of negative rotations, relative to the total number of rotations over a certain period, in this study, 9 years.

$$(3) \qquad LL = (N_{pos} - N_{neg})/(N_{pos} + N_{neg}).$$

We use the nomenclature: LL(x, y) = [-1, 1] for leading- lagging strength: LL (x, y) < 0 implies that y leads x, y→x; LL(x, y) > 0 implies that x leads y, x→y. The LL- strength for the series in Figure 2a is LL = -1. The positive (counter clock-wise) and negative rotations for the paired random series in the upper part of Figure 2 c are shown as positive and negative bars in the lower part

of the figure. A phase plot of the series trajectories is shown in Figure 2d.

The cycle length, CL, of two paired series in Figure 2a is $2\pi \approx 6.28$. The wedge defined by the origin and the points "1" and "2" defines an angle centered in the origin. Summing the angles for all wedges that fill the ellipse gives the angle 2π, and counting the number of points that is required to fill the ellipse with wedges gives n ≈ 6. Generally, there is a correspondence between the cycle length of the paired time series and the rotation of trajectories in the phase plot. The cycle length can be approximated as:

$$(4) \qquad CL = n \times 2\pi / (\sum_2^{n-1} \theta_{i-1,i,i+1}).$$

The cycle times we identify, should ideally be based on (almost) full rotations in the phase plots for the paired time series, but noise, or other superimposed signals may not allow full rotations to be completed as a significant series. The example in Figures 2a and b gives CL = 6.30 which is close to the design cycle time of $2\pi = 6.28$.

Phase shifts, PS. The regression slopes, s, or the β − coefficients, will for cyclic series give information on the shift, or time lag, between the series. For a linear regression applied to paired time series that are normalized to unit standard deviation, the

---

[1] It can be implemented in Excel format: With v_1 = (A1,A2,A3) and v_2 = (B1,B2,B3) in an Excel spread sheet, the angle is calculated by pasting the following Excel expression into C2: =SIGN((A2-A1)*(B3-B2)-(B2-B1)*(A3-A2))*ACOS(((A2-A1)*(A3-A2) + (B2-B1)*(B3-B2))/(SQRT((A2-A1)^2+(B2-B1)^2)*SQRT((A3-A2)^2+(B3-B2)^2))).

regression coefficient, r, and the β – coefficient will be identical. If the two series co-vary exactly, their regression coefficient will be 1, and the time lag zero. If they are displaced half a cycle length, the series are counter-cyclic, and the regression coefficient is r = - 1. Lead or lag times, PS, are estimated from the regression coefficient, r, for sequences of 5 observations, PS (5). With λ as cycle length, an expression for the phase shift between two cyclic series can be approximated by:

(5) $PS \approx \lambda/2\pi \times (\pi/2 - Arcsine(r))$.

For r = 1, Arcsine(r) = π/2, the right hand parenthesis is zero giving PS = 0. For r = -1, arcsine(r) = -π/2 and the right hand parenthesis is 2 × π/2 = π and PS = λ /2.

3.3   Smoothing

We use smoothing for two major purposes. Firstly, we smooth the raw time series to identify long term, multidecadal cyclic patterns, and secondly we smooth the LL- results to emphasize patterns. To smooth the variables we use the LOESS standard smoothing algorithm, SigmaPlot©. The algorithm is available in many statistical packages. The smoothing algorithm has two variables. The first, f, shows how large fraction of the series is used for calculating the running average. The second, p, is the order of the polynomial function used to make interpolations. We always use p = 2. For calculation of LL- relationships, we use two versions of each variable: i) the raw data and ii) LOESS smoothed data with f = 0.3 and p = 2. To emphasize patterns in the figures showing rotational angles, we smooth the raw data, f = 0.3, p = 2.The smoothed curve can be compared visually

to bars that represent the angles based on running average calculations with n = 3. The raw and the smoothed data are subsequently examined with principal component analysis, PCA.

3.4.   Uncertainty estimates

To find an expression for the uncertainty in our estimates we ran Monte Carlo simulations on two paired uniformly random series and found for series n = 9 entries long series that rotations are significant if LL < - 0.32 or LL > + 0.32. The period length, n = 9, is a tradeoff between confidence in the results and the possibility of detecting changing LL-relations. We made all calculations in Excel and with SigmaPlot 12©.

To examine the effect of smoothing and detrending procedures, we smoothed the series for GTA and NAO with a negative exponential smoothing algorithm, and we detrended the same variables with a 4th order polynomial equation, using the residuals as the new detrended variable. The results became essentially the same as with LOESS smoothing.

4. RESULTS

We first examined the variables and their relationship to each other using the principal component analysis, PCA plots. Thereafter, we examined cycle times and phase shifts between the variables. We used both a power spectral density algorithm applied to the single series and the expressions for common cycle times between paired variables, Eq. (4), and for their phase shifts, Eq. (5). Lastly, we examined leading and lagging relationships between the variables using

our algorithm for LL- strength, Eq. (3). The results are explained with reference to the relations between GTA and PDO. We have chosen this pair because the Pacific ocean oscillation, PDO is hypothesized to have a particularly large impact on GTA, e.g., Meehl et al. (2011) and Thompson et al. (2015). Supplementary material 2 shows details of the results for all 6 pairs of the 4 variables.

4.1 Relationships between GTA, CO_2 and ocean oscillation variables.

Principal component, PCA, results for GTA and CO_2 and the three ocean oscillation variables were summarized in the loading and score plots of Figures 1c to f. With raw annual observations, PDO and NAO are correlated and SOI is negatively correlated to both, Figure 1c. GTA and CO_2 are correlated, but relative to ocean currents both variables are either uncorrelated or phase shifted (≈ ¼ cycle time, see discussion). There appears to be a time trend in the series, so that in the long-term states do not repeat themselves, Figure 1e. With smoothed series, that is, with decadal or multidecadal patterns, PDO and SOI are still negatively correlated, but NAO is either uncorrelated or phase shifted relative to the two first ocean oscillations, Figure 1d. The H in Figures 1c and d suggests the position of the hiatus variable in a PCA with the full data set and including the dummy variable for the hiatus periods. However, the PCA shown was made without the hiatus variable.

There are three clusters of system states: 1913 - 1929, 1951 - 1974 and 1993 – 2000, Figure 1f. These clusters correspond fairly well to the reversal times reported for PDO in 1925, 1947 and 1997, (Wu et al. 2011).

4.2 Cycle times and phase shifts

Power spectral density for single variables. We calculate cycle times for single variables by using an algorithm for power spectral density, SigmaPLot©. We apply the algorithm to the raw data and to the LOESS smoothed data with potential cycles in the range 1 to 40 years. Figure 3a shows the results for the raw data and Figure 3b shows the results for the LOESS smoothed data.
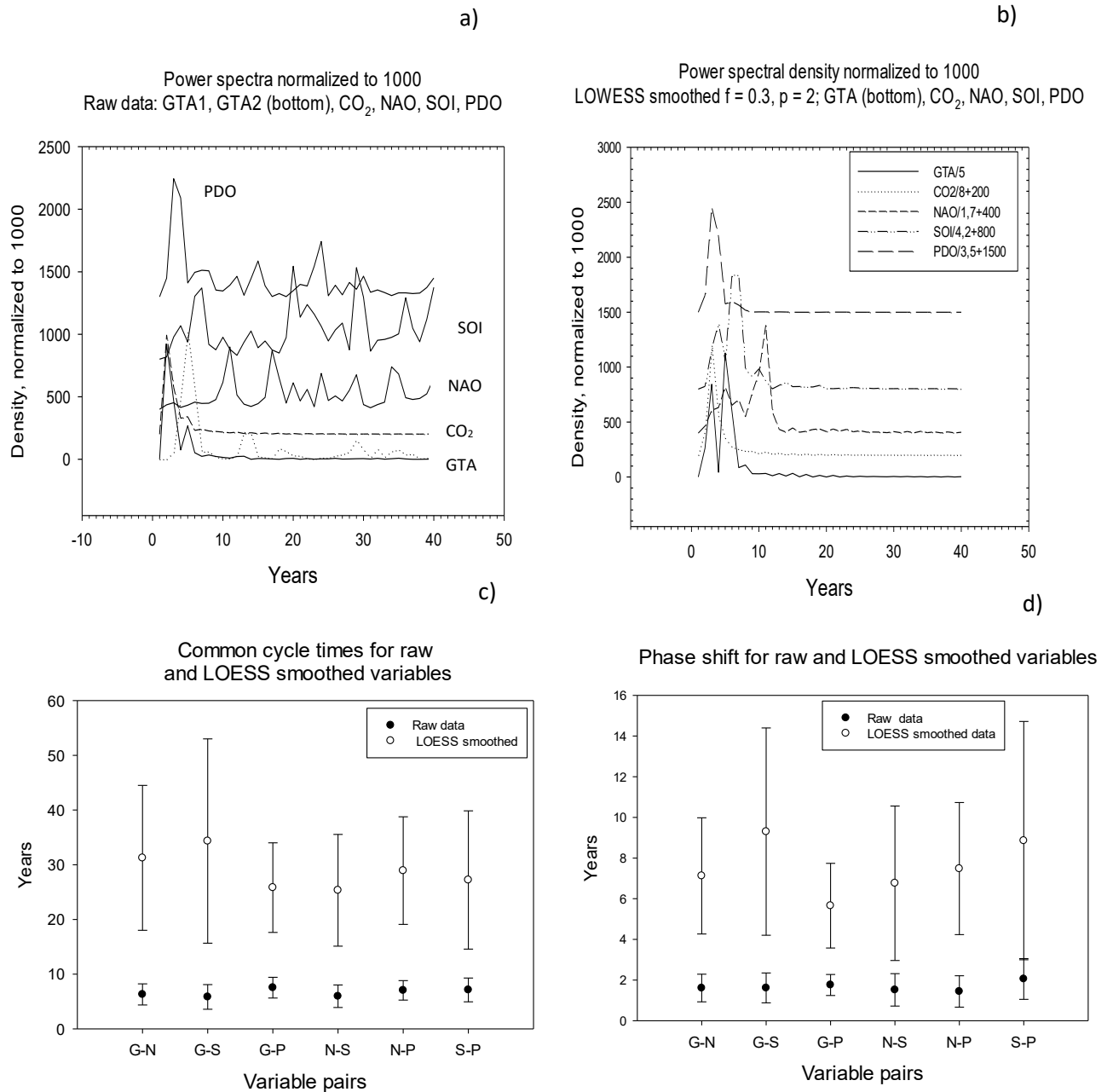
Figure 3. Cycle times for single variables and for paired variables. a) Power spectral density for raw data. Two lower series represent GTA; the smooth series shows the detrended GTA and the wiggling series the raw GTA. Both the raw and the detrended GTA variable have prominent cycles of 5 years, NAO has prominent cycles at 11 and 17 years, SOI has cycles at 7 years and 21 years, and PDO has prominent cycles at 3 years and 7 years. b) Power spectral density for LOESS smoothed data. GTA has a prominent cycle at 5 years, CO_2 has a prominent cycle at 3 years, NAO has a cycle at 5 -7 years and a prominent cycle at 11 years, SOI has a prominent cycle at 6 - 7 years and PDO a prominent cycle at 3 years. c) Common cycle lengths for paired variables, raw and smoothed data; d) Phase shifts for paired variables, raw and smoothed data. Legends are shortened to one letter for clarity: G = Global temperature anomaly, GTA, N = North Atlantic oscillation, NAO; S = Ssouthern oscillation index, SOI; P = Pacific oscillation index, PDO. The standard deviations is for 5 years running average

Cycle times and phase shifts for paired series. Our method allows us to calculate common cycle lengths for paired series. For all pairs we calculated cycle times and phase shifts based on Eqs. (4) and (5). The results based on the raw data and the LOESS smoothed time series for GTA and PDO are shown in Figures 4c and d. The blue shaded areas show periods where cycles are significant. The cycle time for the GTA, PDO pair with annual average values for the significant periods from 1900 to 2000 is 7.5 ± 1.9 years. The phase shift is 1.76 ± 0.5 years. For the smoothed data the cycle time for the significant periods from 1900 to 2000, is 25.8 ± 8.2 and for the phase shift we obtain 7.3 ± 3.2 years. The trends in cycle times and phase shifts were not, or only weakly, significant.

14

Figure 4

a)

Global temperature anomaly and Pacific decadal oscillation, PDO

b)

Global temperature anomaly vs. Pacific decadal oscillation LOESS f = 0.3, p = 2

c)

GTA and PDO: Cycle times and phase shift

d)

GTA vs. PDO: Cycle times and phase shift

e)

Pos. bars GTA leads PDO Neg. bars: GTA lags PDO

f)

Pos bars: GTA leading PDO: Neg. bars GTA lagging PDO
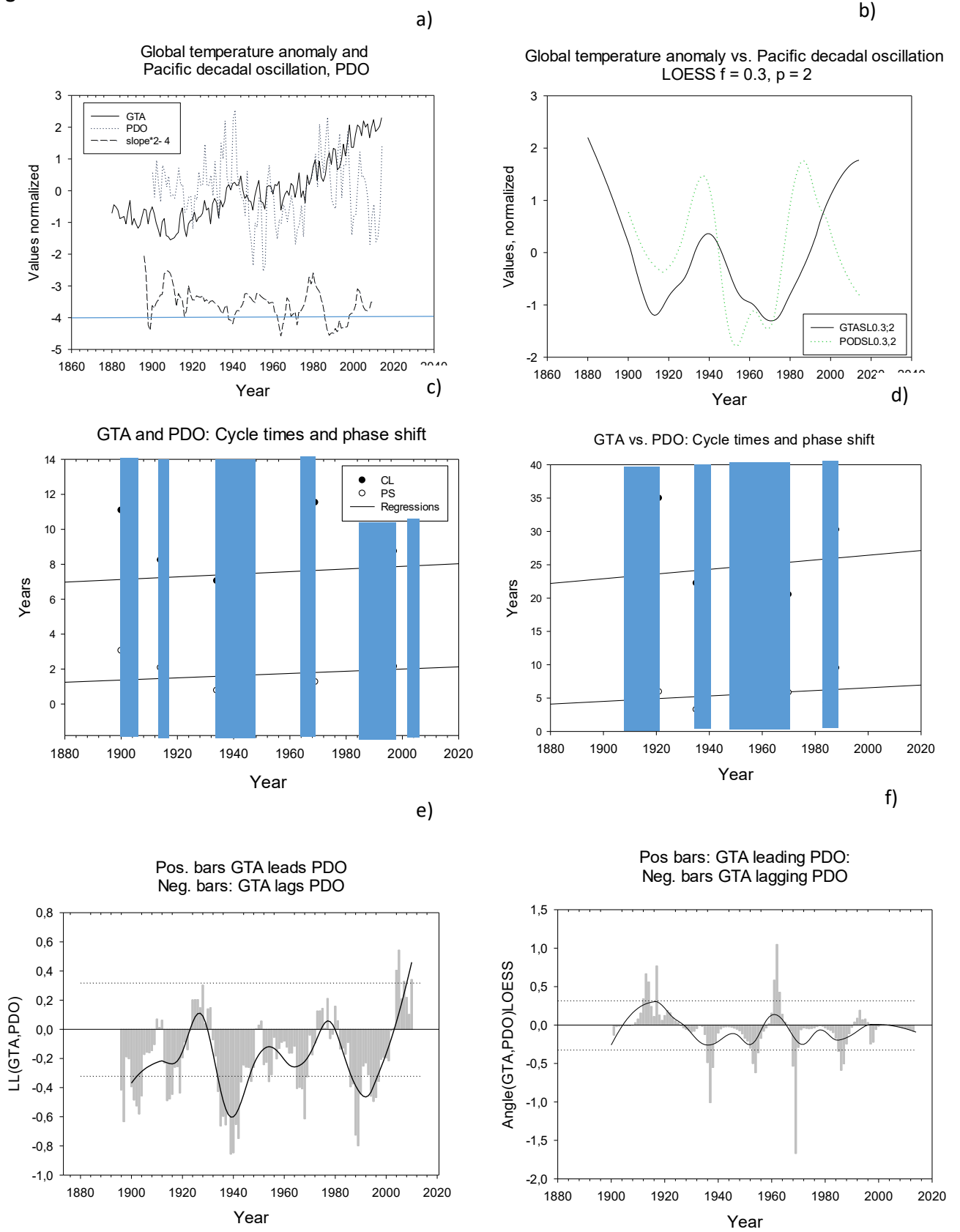
Figure 4. Global temperature anomaly versus Pacific decadal oscillation GTA vs. PDO. Panels in left column: Raw data normalized to unit standard deviation; Panels in right column: LOESS smoothed data normalized to unit standard deviation. a) Raw data (upper two series) and running average (n = 9) β- coefficient (slope) displaced 4 units down, b) LOESS smoothed data, f = 0.3, p = 2, c) Raw data: Cycle times (filled circles) and phase shifts (open circles), d) Smoothed data: cycle time (filled circles) and phase shift (open circles); e) Raw data: LL-relations as angles. Bars are running average (n=3) and line is smoothed values, LOESS, f = 0.3, p = 2   f) Smoothed data: LL- relations as angles. Bars are running average (n=3) and line is smoothed values, LOESS, f = 0.3, p = 2. Blue rectangles indicate significant LL – relations.

The common cycle times for all six pairs were shown in Figure 3c. The average cycle time identified for the 6 pairs of the raw data is 6.6 ± 0.70 years, and for the 6 pairs of LOESS smoothed data is 28.8 ± 3.5 years. Thus, we find two common dominant cycle times in the series, around 7 years and around 28 years.

4.3   Leading lagging relationships between paired series.

We illustrate the leading- lagging, LL-relations with the pair GTA and PDO. The two variables are shown as annual averages in Figure 4a and as smoothed series in Figure 4b. The curves in Figures 4e and f are LOESS smoothed (f = 0.3) and summarize the trends in the LL – relations. With annual average values, we find five periods where GTA is significantly lagging PDO: 1896-1904, 1914 -1919, 1934- 1943, 1965-1969, 1986 – 1997. (We have allowed up to 3 non-significant in-between years). We compare LL-relations among several pairs below.

To identify similarities and differences between LL- relations for the 7 pairs, we show PCA plots for LL- relationships based on the raw data and the smoothed data for the period 1900 to 2000 in Figures 5a and b. In addition to the variables, we have added the dummy variable for the hiatus periods. The explained variance for the principal components is shown in the figures. Adding the values for the hiatus periods will contaminate the pattern for the LL-relations, but the bias turned out to be small.

For both the raw and the smoothed data we outline two major paths that pass through the origin (blue shaded areas). Since the paths are close to perpendicular to each other, this suggests that the cycles in the two sets are shifted a quarter of a cycle length relative to each other. (Perfect sines that are shifted λ/4 to each other will show a circle in the phase plots, giving an explained variance of zero for the scatterplot of sampled sines.) Based on these paths, we depict LL- relations that lie along the same paths, that is, move in approximately the same way, in two plots for the raw data and the two plots for the smoothed data set Figures 5c to f. The LL- relations for the raw data set, identify 7 years cycles and suggest a three to four peak pattern, whereas the LL-relations for the smoothed data set suggest a two-peak pattern. For the two bottom panels e and f we have also added a curve showing the decadal average temperature anomalies following Trenberth (2015).

16

Figure 5   **RAW DATA, Cycle times ≈ 7 years**   **SMOOTHED DATA, cycle times ≈ 25-28 years**
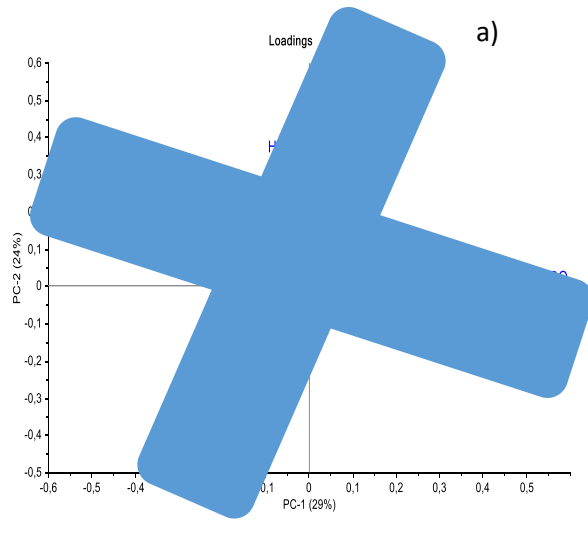
a)

b)

c)

Raw data
Pos. values: First leading second variable
Neg. values: First lagging second variable

d)

LOESS smoothed data
Pos. values: First leading second
Neg. values First lagging second

e)

Raw data
Pos. values: first leading second
Neg. values First lagging second

f)

LOESS smoothed data
Pos. values: First leading second
Neg. values: First lagging second
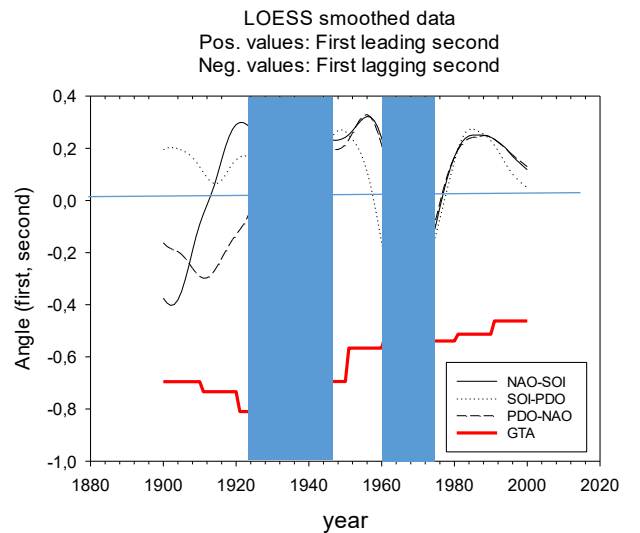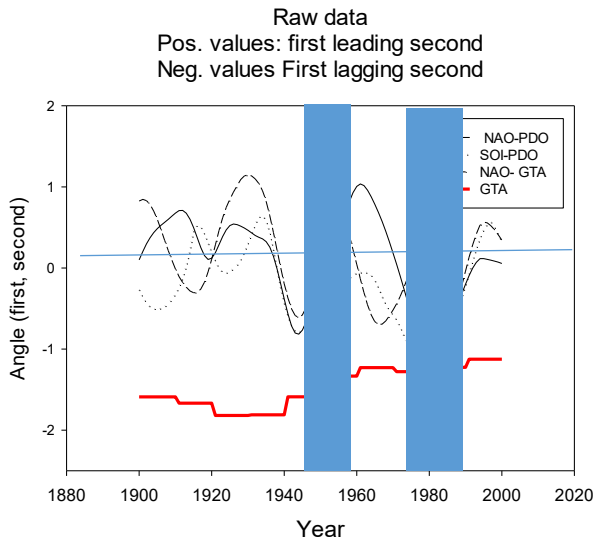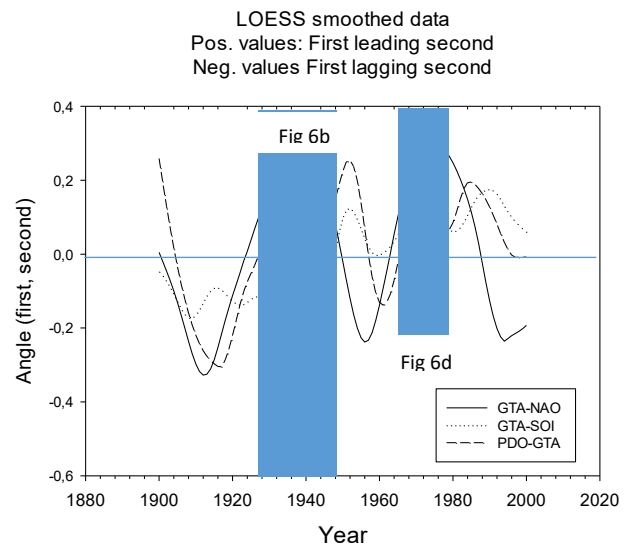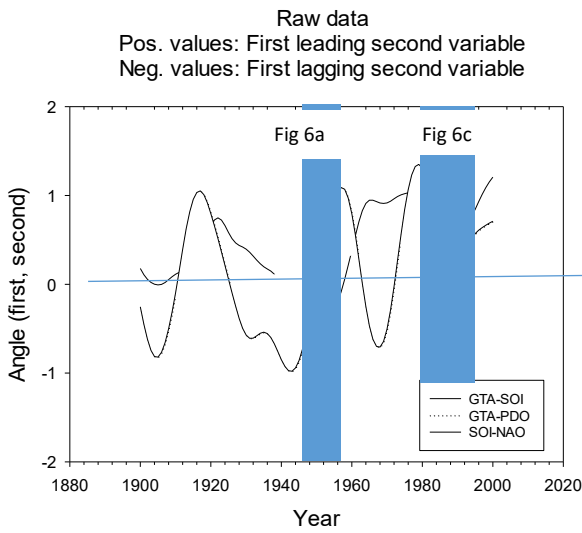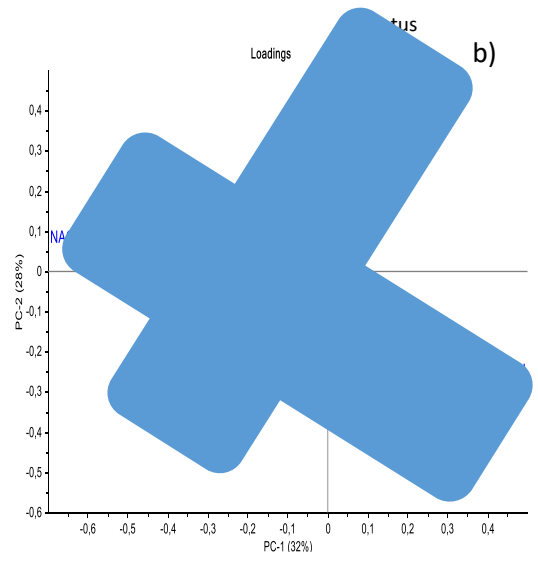
Figure 5. Leading- lagging relationships a) PCA loading plot for LL-relations based on raw data (Cycle lengths are 7.5 ± 1.9 years); b) PCA loading plot for LL- relationships based on LOESS smoothed data (Cycle lengths are 28 ± 10 years; c) Three LL- relations (based on raw data) that correlate (NAO -SOI with negative sign). d) Three LL- relations (based on LOESS smoothed data) that correlate (GTA - PDO with negative sign); e) Three LL- relations (raw data) that correlate (GTA - NAO with negative sign); f) Three LL- relations (LOESS smoothed data) that correlate (NAO - PDO with negative sign). Shaded areas suggest periods with consistent LL -relations. Note that the smoothed LL- relations are based on the full series from 1880 to 2014, except the PDO series that start in 1900. For the PCA plots, we restrict the series to the period 1900 to 2000 to avoid end-effects.

For the 7 years cycle during the period 1940 to 1950 and the 25- 28 years cycle during the period 1930 to 1945, Figures 5c and d, the LL- patterns can be depicted as in Figures 6a and b. The variables in Figure 6 are arranged so that the NAO is to the West (left), the PDO to the East (right) and the SOI at the bottom, corresponding roughly to their position on a map with Europe- Africa in the middle. GTA is at the top. For the 25-28 years cycles preceding the big hiatus 1943- 75, we obtain the sequence GTA → NAO → SOI → PDO → GTA. It is a circular LL-relationship. We also find that PDO precedes NAO, and SOI precedes GTA. To get from the curves in Figure 5 to the directional graphs in Figure 6, the directions can be read from the graphs according to the heading at the top of the panels.

Figure 6

a)

b)

7 year cycle ≈ 1940-50;

25 years cycle ≈ 1930 - 1945

Y = SOI

X = NAO

Counter clock-wise rotation: X→ Y x ; NAO → SOI

c)

d)

7 years cycle ≈ 1970-90

25 years cycle 1970 -80
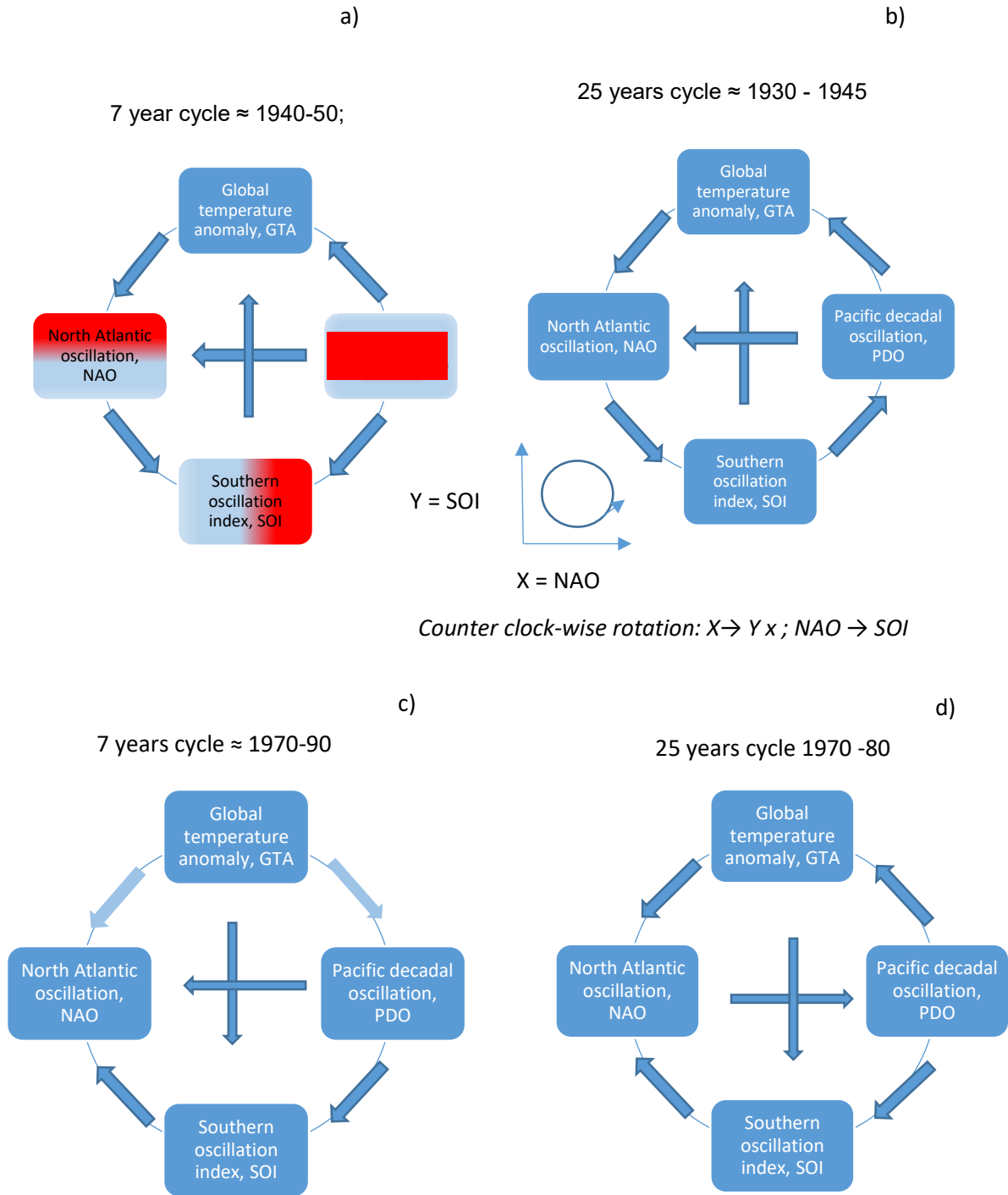
Figure 6. Leading- lagging, LL- relations between GTA and three ocean oscillation variables (proxies for the "ocean currents"). To get from the time series in Figure 5c to f to the sequential patterns in Figure 6, the inset coordinate system in Fig 6 may be helpful. Assign the first variable to the x-axis and the second variable to the y-axis. If the rotation is positive (counter clock-wise), we have x → y. a) Sequences for the seven years cycles during the

period 1940 – 50. Colors suggest regionally high temperature anomalies when the indexes have a high value. b) Sequences for the 25 years cycles during the period 1930 to 1945.. c) Sequences for the 7 years cycle during 1970-90, d) Sequence for the 25 years cycle during the period 1970 to 1980. Although there are exceptions, the LL- relations appear to change in concert. Light shaded arrows suggest weak LL- relations.

However, for the period 1970 to about 1990 the LL- patterns for the 7 years cycle seem to start with global temperature, GTA, preceding both NAO and PDO, although weakly. Then we get PDO → SOI → NAO as shown in Figure 6c. Figure 6d shows that the 25 years cycle is different. Global temperature anomaly still affects NAO, GTA → NAO, but now the Pacific decadal oscillation affects GTA, PDO → GTA. However, PDO also affects SOI, and SOI again affects NAO.

4.4 The hiatus periods.

We do not find a significant relationship between the hiatus periods and LL-relations for the ocean currents in the raw data set. However, for the smoothed variables, Figures 5b, d and f, the bimodal pattern is more pronounced, and the relationships between the Hiatus period and LL(GTA,SOI), LL(GTA,NAO) and – LL(GTA,PDO) are stronger, but not significant.

5. DISCUSSION

We first discuss our results on ocean oscillations and teleconnections. Thereafter we discuss possible implications for pauses in global warming, the hiatus periods. Thirdly, we discuss the two cycle frequencies we find for ocean oscillations and compare them to frequencies found in other studies. Fourthly, we try to identify mechanisms that cause cycles in one ocean basin to impact cycles in another ocean basin, that

is "bridges" for interferences between ocean water bodies. Lastly, we discuss the leading –lagging method and its application to atmospheric and ocean variables.

5.1 Ocean oscillations and teleconnections

We find that leading and lagging relations between ocean current oscillations change direction in concert. Assuming that the LL-relations correspond to cause – effect, we can infer several interaction patterns among the ocean oscillation variables. (Possible causal mechanisms will be discussed in section 5.5.) When one interaction pattern changes, there are corresponding changes also in the other interaction patterns, Figures 5 a to f. The results support our *first* hypothesis that the large ocean currents interact in concert, partly supporting the teleconnection hypothesis. However, whereas there is a circular LL- sequence before 1960s, global warming appears to exert a larger influence on the LL-relations after the 1960s. This finding corresponds with climate modeling evidence for an increasing frequency of extreme El Niño events due to greenhouse warming found by Cai et al. (2015), and with an apparent breakpoint in oscillation volatility in 1960 found by Torrence and Webster (1999) and Kestin et al. (1998). Wang et al. (2013) suggest that greenhouse gases are increasingly important precursors to the ENSO after

1960s. A more concerted movement in IPO, SOI and El Niño after 1945 was found by Power et al. (2006). Loeb et al. (2012) and Johnson et al. (2016) found that on an interannual time scale 2001-2011, ENSO events lead to potentially large perturbations in the top of the atmosphere, TOP, radiation.

Wu et al. (2011) discuss leading- lagging relations between PDO and the Atlantic multidecadal oscillation, AMO. They found that on an interannual time scale (< 10 years, corresponding to our 7 years cycles), PDO leads the AMO by 1 year, but on a multidecadal time scale (> 10 years, corresponding to our 25 years cycles) AMO leads PDO by 11 -12 years. These results are consistent with our findings except that we find a shorter lead-time of 7 years for the multidecadal cycles. We compare raw and smoothed data for NAO, AMOC and AMO in supplementary material 1.

5.2 Hiatus periods and global temperature change

There are two large scale ocean circulation systems that have been hypothesised to be major parts of the heat engine of the global climate system, the PDO, (Meehl et al. 2011) and the Atlantic meridional overturning circulation, AMOC (McCarthy et al. 2015). A summary is given in Hedemann et al. (2017)

The hiatus periods. The slowdown in the rate of global warming in the early 2000 as well as a slowdown in the period 1943 to about 1975 (and probably also the period 1902-20) have been associated with storing of heat in the deep oceans (depth > 700 m), Trenberth (2015), Meehl et al.

(2011), and Meehl et al. (2014). The hiatus periods seem to be most closely related to the 25-28 years cycle, Figure 5b. The hiatus periods occur when GTA leads SOI, and NAO, but PDO leads GTA. In spite of results not being significant at the 0.05 level, it is interesting to compare them to findings in other studies. GTA leading SOI means that GTA peaks about 7 years before the SOI peaks. If we "translate" the SOI peak into regional sea surface temperature, SST, we find that an increase in GTA is followed about 7 years later by abnormally warm waters across the tropical Pacific, typical of El Niño episodes, but with colder sea surface temperatures near 30° to 40° N and S latitude in the Pacific and Atlantic, Meehl et al. (2011), on SST.

Our results also suggest that PDO is a leading variable to GTA during hiatus periods. In terms of GTA and SST, this suggests that an increase in the average SST over the tropical Pacific, (PDO increases) and a colder-than-average temperature in the northwest and southwest Pacific is followed about 7 years later by an increase in the GTA. This corresponds well with results by Meehl et al. (2014), Trenberth (2015) and Dai et al. (2015) that a positive phase of PDO increases the global average sea surface temperature. The leading time has been reported to be about 7 years. Thus, ocean heath transfer may compensate for an increase in GTA caused by CO_2 and thus contributes to a hiatus period. This supports our *second* hypothesis, that the hiatus periods are associated with particular events in the ocean current cyclic system. However, there are only 3

entries available for the hiatus periods, so the results should be treated with caution.

The AMO, the AMOC and NAO share the same general time series pattern but peaks and troughs are shifted in time, and the AMOC shows a generally decreasing trend. The recent slowdown in AMOC has been hypothesized to cause a cooling over the northwest Europe, (Bryden et al. 2005) which has been compensated by greenhouse warming (Thornalley et al. 2018). Thus, both PDO (our results) and the AMOC may compensate for greenhouse warming. In addition, changes in the AMOC have been associated with the seesaw effect, that is, temperature changes in the southern and northern hemisphere are out of phase (Stocker and Johnsen 2003). Results by Yao et al. (2017) higlight the importance of multiple oceans on the multi-decadal global warming rates. Hedemann et al. (2017), however, suggest that it is not possible to entangle contributions to the hiatus from oceans and from changes in radiative flux imbalances at the top of the atmosphere, TOA.

The effects of both ocean warming and greenhouse gases may also help explain the puzzle that global temperature leads CO_2 during the period from about 1960 to 2003, (Kuo et al. 1990; Seip and Grøn 2017).

5.3   Data interpretation.
The time series we analyze are frequently used proxies for oscillations in ocean system variables. We here tacitly assume that the series represent large ocean currents, although two of the series, SOI and NAO, measure atmospheric phenomena and one series measures sea surface temperature, PDO. To our knowledge, there are no systematic survey of leading – lagging relationships between global ocean oscillation variables like NAO, SOI and PDO, and water movements, or variations in regional temperature anomalies. The two variables, AMOC and AMO measure more complicated aspects of the Atlantic ocean; AMOC measures the net effect of surface and subsurface flows and AMO is an area averaged areal measure. A study of the three Atlantic ocean time series, NAO, AMOC and AMO, however, are outside the scope of the present study.

5.3.1   Smoothing
It is customary to smooth the raw time series data both to remove noise and to identify underlying cycles in the observed time series. There are several ways to smooth the data for ocean currents. For example, Chylek et al. (2014 a) used 5 years moving averages and Caesar et al. (2018) uses a 20 years locally weighted LOWESS smoothing. Our series are smoother than those presented by Chylek et al. (2014 a), their Figure 2, but show a similar pattern in the period 1900 to 2000. Our smoothed series for PDO show the same periods with positive values as the IPO series used by Meehl et al. (2014), that is, negative in the periods 1960 - 80 and 1998 - 2010 and positive in the period 1980 -98. The inverse relationships we find between SOI and PDO for both the annually averaged values and the smoothed values correspond with the relationships found by Finlay et al. (2015) in their study of hardwater lakes and atmospheric warming. Positive values of

NAO and SOI are associated with positive temperature anomalies in central North America. We find that the hiatus periods correlate with SOI and – (minus) PDO in agreement with the result of Meehl et al. (2011) and Trenberth (2015).

5.4   Cycle time and phase shifts

We found 6 to 7 years cycles in the raw data and 25-28 years cycles in the smoothed series both in all single series by applying the Power spectral density algorithm, and with our algorithm for identifying common cycles for paired series.

To partly validate the chronology in LL-relations we compare the timing of changes in LL-relations to tie events; either to endogenous events (for example the El Niño 1997/98 extreme event) or to events identified by other authors.

5.4.1 The 7 years cycles.

There are several findings that support the years 1916, 1942, 1957, 1967 and 1980 identified as turning points in our 7-years cycles as tie events in teleconnection studies. i) The peak and troughs in the LL-relations are found for many pairs, also for pairs that do not share a common ocean oscillation variable. ii) The years coincide well with the years found by Swanson and Tsonis (2009) for synchronization of variables of the Northern Hemisphere climate system (ENSO, PDO, NAO, The North Pacific index), with years for regime shifts or alternating polarity in the Pacific sector around 1920, 1940 and 1976/77 found by Minobe (1997) and an identification of regime shifts in 1920, 1940, 1970 and around 2000 found by Chen and Wallace (2015). Lastly, it

corresponds with the finding of global impacts of regime shifts in the 1980s by Reid et al. (2016). iii) Kestin et al. (1998) found a range of cycle times, but with particularly high power around 3-4 years and 7 to 10 years. They also identified 5 periods with short cycles of 2.4 years, and 4 of these correspond with years where we find short cycles. (However, Kestin et al. (1998) attribute these cycles to poor time localization.) iv) We have found two studies that suggest that there are changes in East - West propagation of the ENSO (Zhang et al. 1998; Zhu et al. 2011). These two last studies also use subsurface temperature anomalies.

5.4.2 The 25 – 28 years cycles

For the smoothed variables, we obtained a consistent cycle time of about 25 - 28 years. The 25 - 28 years period is longer than the 20 years period for the interdecadal pacific oscillation, IPO identified by Meehl et al. (2014), their Figure 2 or the 23 year cycle, 1661 to the present, identified by Biondi et al. (2001). Torrence and Webster (1999), using wavelet analysis, also found cycle times in the range 20 – 30 years. There may also be cycles that are much longer, but our period 1880 to 2014 is too short to identify such cycles. The studies referred to above use different techniques to analyze climate time series, suggesting that the information found in the series are not artefacts of the methods.

Thus, our *third hypothesis* was partially supported, we found cycles that also could be found in the single variables, but only the two sets 6 - 7 and 25 - 28 years cycles were carried over between ocean

currents. However, cycles shorter than about 5 years may be an apparent pattern caused by stochastic movements between paired series (Seip and Grøn 2017 b).

5.5 Candidate causal mechanism, "bridges".

By pairing ocean cycle series we find that cycles in one ocean water body impact cycles in another, neighbouring ocean water body. "Bridges" that facilitate transport of warm, or cold waters and air have been identified in the literature, e.g., Zhang et al. (1998) on subsurface ocean "bridges", Yao et al. (2016) on atmospheric "bridges". There may also exist a common factor which influences two, or all three currents, discussed in this study, (Graham et al. 2011).

Meehl et al. (2015) relate a cooling incident over U.S. to a transition in the interdecadal Pacific Oscillation, IPO. Davis et al. (2011) show that wind stress magnitude during the period 1980 -2005 correlates with the PDO index and with basin scale wind, and that the latter is leading the PDO index (SST) by 3 months. They also show that the basin scale air – heath exchange correlates with the PDO, and that there is zero time lag between wind stress and net heat flux. Durski et al. (2015) show that the near coastal alongshore surface currents show seasonal variability which mostly corresponds to that expected from response to wind stress. Kestin et al. (1998) show that the cycle – year state of SOI, SST and equatorial rainfall capture the same phenomena.

There are also some studies that address reversals in circulation or flow directions.

Graham et al. (2011) summarize indications for historic shifts in global circulation patterns. During the period 1976 - 77, an apparent reversal of polarity began to occur with changes in circulation pattern in the Pacific. (Zhang et al. 1998). Around 1975-82 the ENSO was initiated in the South American coast and propagated westward along the equator (Zhu et al. 2011). This may fit with SOI leading NAO during the period 1970-1980 both over short (7 years) and long (25 years) cycles. However, around 1980, the long cycles for SOI ceased to lead NAO (Fig 5f), and in 1982 el Niño was reported to propagate eastward from the central basin (Zhu et al. 2011).

5.6 The LL- method

Our LL-strength method distinguishes itself from other methods, e.g., cross spectral methods, cross correlation methods, (Granger 1969) to identify LL-relations, cycle lengths and phase shifts in that it is local. LL-relations can be determined with n > 3, but require longer series, e.g., n ≈ 9, to allow calculation of confidence estimates. Alternative methods that we are aware of require observational time series of sufficient duration to enable stable spectra, (Gehne et al. 2014). Kestin et al. (1998) use 3 methods that are based on fixed 21 year windows or on adaptive windows (range ≈ 10 to 50 years).

Most often a peak in one variable which is closely before the peak in a second variable, is interpreted to mean that there is a causal effect from the first to the last variable. (Hartmann 2016). However, the variables may affect each other, but the

time it takes for the effects to act is longer than half their common cycle times. Therefore, an alternative interpretation is that the second variable is affecting the first, but with a long time delay, (> ½ cycle length). For the oceanic oscillations studied here, this is a possibility. Incorporating more teleconnections into the system studied, e.g., like Tasambay-Salazar et al. (2015), may help tightening relations and help confirm real causal relations.

We believe that the method used in the present paper is robust for most cyclic time series, in particular with regard to LL-relations. However, there are several challenges that should be addressed further. Noise, as well as superposition of cycles with different cycle lengths (and opposite LL- relations) may bias the results, as is the case for all alternative methods. However, if contaminations of the signals are too great, the LL- strength measure will show that the series, or portions of the series, are non-significant. Furthermore, cycles longer than 6 years have a probability less than $p = 0.05$ to occur by chance, suggesting that cycles 7 years or longer are real. Our study is not addressing dynamic explanations, which is outside the scope of the present study.

We tested other methods for detrending (4th order polynomial) and smoothing (negative exponential), and the results were similar. Se supplementary material 3. We believe that the new method would be very useful if it is applied together with simulation models for global temperature, wind and ocean currents.

6. CONCLUSION

We find interaction patterns between global temperature change and proxies for three major ocean variables, the north Atlantic oscillation, NAO, the southern oscillation index, SOI (related to La Niña and El Niño) and the Pacific decadal oscillation, PDO.

We found two dominant cycle times in the temperature/ ocean current system, one 6 - 7 years cycle and one 25 - 28 years cycle. Global temperature and the three ocean oscillations show concerted interactions. Before about 1960 the 25-28 years ocean oscillations showed a circular sequence GTA → NAO→ SOI → PDO → GTA. During the period 1970-80 this pattern changed. After about 1970, the superimposed 7-years cycle appears to be dominated by GTA, but not significantly. Thus, the years around 1960 may be a break point in oceanic teleconnections. The slowdown in temperature increase which occurs during the hiatus periods is closely associated with periods where GTA is a leading variable to SOI. Increases in GTA will cause typical El Niño episodes with warm waters across the tropical Pacific, but colder water North and South. The results for cycle times, phase shifts and leading – lagging relations were calculated as running averages over 3 to 9 years. This made it possible to identify patterns in the variation of the major ocean variables by the LL- method that will be hidden when LL- relations based on averages over longer time series are examined.

resources required to complete this paper.
For both authors there are no conflict of
interests.

Literature

Biondi, F., A. Gershunov and D. R. Cayan. 2001. North Pacific decadal climate variability since 1661. Journal of Climate 14(1): 5-10.

Bryden, H. L., H. R. Longworth and S. A. Cunningham. 2005. Slowing of the Atlantic meridional overturning circulation at 25 degrees N. Nature 438(7068): 655-657.

Caesar, L., S. Rahmstorf, A. Robinson, G. Feulner and V. Saba. 2018. Observed fingerprints of weakening Atlantic Ocean overturning circulation. Nature 556(191-196).

Cai, W. J., G. J. Wang, A. Santoso, M. J. McPhaden, L. X. Wu, F. F. Jin, A. Timmermann, M. Collins, G. Vecchi, M. Lengaigne, M. H. England, D. Dommenget, K. Takahashi and E. Guilyardi. 2015. Increased frequency of extreme La Nina events under greenhouse warming. Nature Climate Change 5(2): 132-137.

Chen, X. Y. and J. M. Wallace. 2015. ENSO-Like Variability: 1900-2013. Journal of Climate 28(24): 9623-9641.

Chylek, P., M. K. Dubey, G. Lesins, J. N. Li and N. Hengartner. 2014 a. Imprint of the Atlantic multi-decadal oscillation and Pacific decadal oscillation on southwestern US climate: past, present, and future. Climate Dynamics 43(1-2): 119-129.

Dai, A. G., J. C. Fyfe, S. P. Xie and X. G. Dai. 2015. Decadal modulation of global surface temperature by internal climate variability. Nature Climate Change 5(6): 555-559.

Davis, X. J., L. M. Rothstein, W. K. Dewar and D. Menemenlis. 2011. Numerical Investigations of Seasonal and Interannual Variability of North Pacific Subtropical Mode Water and Its Implications for Pacific Climate Variability. Journal of Climate 24(11): 2648-2665.

Duchez, A., J. J. M. Hirsch, S. A. Cunningham, A. T. Blaker, H. L. Bryden, B. de Cuevas, C. P. Atkinson, G. D. McCarthy, E. Frajka-Williams, D. Rayner, D. Smeed and M. S. Mizielinski. 2014. A New Index for the Atlantic Meridional Overturning Circulation at 26 degrees N. Journal of Climate 27(17): 6439-6455.

Durski, S. M., A. L. Kurapov, J. S. Allen, P. M. Kosro, G. D. Egbert, R. K. Shearman and J. A. Barth. 2015. Coastal ocean variability in the US Pacific Northwest region: seasonal patterns, winter circulation, and the influence of the 2009-2010 El Nio. Ocean Dynamics 65(12): 1643-1663.

Finlay, K., R. J. Vogt, M. J. Bogard, B. Wissel, B. M. Tutolo, G. L. Simpson and P. R. Leavitt. 2015. Decrease in CO_2 efflux from northern hardwater lakes with increasing atmospheric warming. Nature 519(7542): 215-218.

Gehne, M., R. Kleeman and K. E. Trenberth. 2014. Irregularity and decadal variation in ENSO: a simplified model based on Principal Oscillatory Petterns. Clim Dyn.

Graham, N. E., C. M. Ammann, D. Fleitmann, K. M. Cobb and J. Luterbacher. 2011. Support for global climate reorganization during the "Medieval Climate Anomaly". Climate Dynamics 37(5-6): 1217-1245.

Granger, C. W. J. 1969. Investigating Causal Relations by Econometric Models and Cross-spectral Methods. Econometrica, 37(3): 423-438.

Hartmann, D. L.2016). "Objective Analysis." 2016, from http://www.atmos.washington.edu/~dennis/552_Notes_ftp.html.

Hedemann, C., T. Mauritsen, J. Jungclaus and J. Marotzke. 2017. The subtle origins of surface-warming hiatuses. Nature Climate Change 7(5): 336-+.

Hurrell, J. W. 1995. Decadal Trends in the North-Atlantic Oscillation - Regional Temperatures and Precipitation. Science 269(5224): 676-679.

Johnson, G. C., J. M. Lyman and N. G. Loeb. 2016. CORRESPONDENCE: Improving estimates of Earth's energy imbalance. Nature Climate Change 6(7): 639-640.

Keeling, C. D. and T. P. Whorf. 1997. Possible forcing of global temperature by oceanic tides. Proc. Natl. Acad. Sci. USA 94: 8321-8328.

Kestin, T. S., D. J. Karoly, J. I. Yang and N. A. Rayner. 1998. Time-frequency variability of ENSO and stochastic simulations. Journal of Climate 11(9): 2258-2272.

Kuo, C., C. Lindberg and D. J. Thomson. 1990. Coherence Established between Atmospheric Carbon-Dioxide and Global Temperature. Nature 343(6260): 709-714.

Loeb, N. G., J. M. Lyman, G. C. Johnson, R. P. Allan, D. R. Doelling, T. Wong, B. J. Soden and G. L. Stephens. 2012. Observed changes in top-of-the-atmosphere radiation and upper-ocean heating consistent within uncertainty. Nature Geoscience 5(2): 110-113.

Luterbacher, J., E. Xoplaki, D. Dietrich, R. Rickli, J. Jacobeit, C. Beck, D. Gyalistras, C. Schmutz and H. Wanner. 2002. Reconstruction of sea level pressure fields over the Eastern North Atlantic and Europe back to 1500. Climate Dynamics 18(7): 545-561.

Lynch-Stieglitz, J. 2017. The Atlantic Meridional Overturning Circulation and Abrupt Climate Change. Annual Review of Marine Sciences, Vol 9 9: 83-104.

Mazzarella, A. and N. Scafetta. 2012. Evidences for a quasi 60-year North Atlantic Oscillation since 1700 and its meaning for global climate change. Theoretical and Applied Climatology 107(3-4): 599-609.

McCarthy, G. D., I. D. Haigh, J. J. M. Hirschi, J. P. Grist and D. A. Smeed. 2015. Ocean impact on decadal Atlantic climate variability revealed by sea-level observations. Nature 521(7553): 508-U172.

McCarthy, G. D., D. A. Smeed, W. E. Johns, E. Frajka-Williams, B. I. Moat, D. Rayner, M. O. Baringer, C. S. Meinen, J. Collins and H. L. Bryden. 2015. Measuring the Atlantic Meridional Overturning Circulation at 26 degrees N. Progress in Oceanography 130: 91-111.

McPhaden, M. J. 1999. Genesis and evolution of the 1997-98 El Nino. Science 283(5404): 950-954.

Meehl, G. A., J. M. Arblaster and C. T. Y. Chung. 2015. Disappearance of the southeast US "warming hole" with the late 1990s transition of the Interdecadal Pacific Oscillation. Geophysical Research Letters 42(13): 5564-5570.

Meehl, G. A., J. M. Arblaster, J. T. Fasullo, A. X. Hu and K. E. Trenberth. 2011. Model-based evidence of deep-ocean heat uptake during surface-temperature hiatus periods. Nature Climate Change 1(7): 360-364.

Meehl, G. A., H. Y. Teng and J. M. Arblaster. 2014. Climate model simulations of the observed early-2000s hiatus of global warming. Nature Climate Change 4(10): 898-902.

Minobe, S. 1997. A 50-70 year climatic oscillation over the North Pacific and North America. Geophysical Research Letters 24(6): 683-686.

NASA(GISTEMP).2014). "GISS Surface Temperature Analysis (GISTEMP)." 2014, from http://data.giss.nasa.gov/gistemp.

Nieves, V., J. K. Willis and W. C. Patzert. 2015. Recent hiatus caused by decadal shift in Indo-Pacific heating. Science 349(6247): 532-535.

Power, S., M. Haylock, R. Colman and X. D. Wang. 2006. The predictability of interdecadal changes in ENSO activity and ENSO teleconnections. Journal of Climate 19(19): 4755-4771.

Reid, P. C., R. E. Hari, G. Beaugrand, D. M. Livingstone, C. Marty, D. Straile, J. Barichivich, E. Goberville, R. Adrian, Y. Aono, R. Brown, J. Foster, P. Groisman, P. Helaouet, H. H. Hsu, R. Kirby, J. Knight, A. Kraberg, J. P. Li, T. T. Lo, R. B. Myneni, R. P. North, J. A. Pounds, T. Sparks, R. Stubi, Y. J. Tian, K. H. Wiltshire, D. Xiao and Z. C. Zhu. 2016. Global impacts of the 1980s regime shift. Global Change Biology 22(2): 682-703.

Salinger, M. J., J. A. Renwick and A. B. Mullan. 2001. Interdecadal Pacific Oscillation and South Pacific climate. International Journal of Climatology 21(14): 1705-1721.

Seip, K. L. 2015. Investigating possible causal relations among physical, chemical and biological variables across regions in the Gulf of Maine. Hydrobiologia 744: 127-143.

Seip, K. L. and Ø. Grøn. 2017. A new method for identifying possible causal relationships between CO_2, total solar irradiance and global temperature change. Theoretical and Applied Climatology 127: 923-938.

Seip, K. L. and Ø. Grøn. 2017. On the statistical nature of distinct cycles in global warming variables. Climate dynamics.

Stocker, T. F. and S. J. Johnsen. 2003. A minimum thermodynamic model for the bipolar seesaw. Paleoceanography 18(4).

Swanson, K. L. and A. A. Tsonis. 2009. Has the climate recently shifted? Geophysical Research Letters 36.

Tasambay-Salazar, M., M. J. OrtizBevia, F. J. Alvarez-Garcia and A. M. RuizdeElvira. 2015. An estimation of ENSO predictability from its seasonal teleconnections (vol 122, pg 383, 2015). Theoretical and Applied Climatology 122(1-2): 401-401.

Thompson, D. M., J. E. Cole, G. T. Shen, A. W. Tudhope and G. A. Meehl. 2015. Early twentieth-century warming linked to tropical Pacific wind strength. Nature Geoscience 8(2): 117-121.

Thornalley, D. J. R., D. W. Oppo, P. Ortega, J. I. Robson, C. M. Brierley, R. Davis, I. R. Hall, P. Moffa-Sanchez, N. L. Rose, P. T. Spooner, I. Yashayaev and L. D. Keigwin. 2018. Anomalously weak Labrador Sea convection and Atlantic overturning during the past 150 years. Nature 556(7700): 227-+.

Thornalley, D. R., D. W. Oppo, P. Ortega, J. I. Robson, C. M. Brierley, R. Davis, I. R. Hall, P. Moffa-Sanchez, N. L. Rose, P. T. Spooner, I. Yashayaev and L. D. Keigwin. 2018. Anomalously weak Labrador sea convection and Atlantic overturning during the past 150 years. Nature 556: 227-232.

Torrence, C. and P. J. Webster. 1999. Interdecadal changes in the ENSO-monsoon system. Journal of Climate 12(8): 2679-2690.

Trenberth, K. E. 2015. Has there been a hiatus? Science 349(6249): 691-692.

Trenberth, K. E. and J. T. Fasullo. 2013. An apparent hiatus in global warming? Earths Future 1(1): 19-32.

Wang, S. Y., M. L'Heureux and J. H. Yoon. 2013. Are Greenhouse Gases Changing ENSO Precursors in the Western North Pacific? Journal of Climate 26(17): 6309-6322.

White, W. B. and D. R. Cayan. 1998. Quasi periodicity and global symmetries in interdecadal upper ocean temperature variability. J. Geophys.Res. 103: 21335-21354.

Wu, S., Z. Y. Liu, R. Zhang and T. L. Delworth. 2011. On the observed relationship between the Pacific Decadal Oscillation and the Atlantic Multi-decadal Oscillation. Journal of Oceanography 67(1): 27-35.

Yao, S.-L., G. Huang, R.-G. Wu and X. Qu. 2016. The global hiatus - a natural product of interactions of a secular warming trend and a multi-decadal oscillation. Theor. Appl. climatol 123: 349-360.

Yao, S. L., J. J. Luo, G. Huang and P. F. Wang. 2017. Distinct global warming rates tied to multiple ocean surface temperature changes. Nature Climate Change 7(7): 486-+.

Zhang, L. P. and C. Z. Wang. 2013. Multidecadal North Atlantic sea surface temperature and Atlantic meridional overturning circulation variability in CMIP5 historical simulations. Journal of Geophysical Research-Oceans 118(10): 5772-5791.

Zhang, R. H., L. M. Rothstein and A. J. Busalacchi. 1998. Origin of upper-ocean warming and El Nino change on decadal scales in the tropical Pacific Ocean. Nature 391(6670): 879-883.

Zhen-Shan, L. and S. Xian. 2007. Multi-scale analysis of global temperature changes and trend of drop in temperature in the next 20 years. Meterol. Atmos. Phys. 95: 115-121.

Zhu, J., G. Zhou, R. H. Zhang and Z. Sun. 2011. On the role of oceanic entrainment temperature (T-e) in decadal changes of El Nino/Southern Oscillation. Annales Geophysicae 29(3): 529-540.